Design and Experiment of Magnetic Periodic Reversal Spring for Torque Ripple Suppression of AC Motors

Haruaki Ito
Graduate School of Science and Engineering
Ibaraki University
Hitachi, Japan
24nm606x@vc.ibaraki.ac.jp

Masayuki Kato
Graduate School of Science and Engineering
Ibaraki University
Hitachi, Japan
masayuki.kato.actuator@vc.ibaraki.ac.jp

***Abstract*—Various methods have been investigated to suppress torque ripple of interior permanent magnet synchronous motors (IPMSM). However, all of these methods have disadvantages. To address this issue, the authors have proposed a new passive torque ripple suppression method for AC motors using the magnetic periodic reversal spring (MPRS). However, previous research only evaluated this method based on static torque characteristics in an ideal environment. Therefore, this paper reports the results of a more detailed evaluation of its practicality. Three-dimensional finite element analysis revealed that the MPRS eddy current loss is extremely small, approximately 0.04% of the IPMSM iron loss, indicating that motor efficiency is not affected. Additionally, the radial force amplitude was found to be low, about 6% of the IPMSM's, predicting a minimal increase in vibration and noise due to MPRS integration. Furthermore, experimental verification was conducted. Although the static torque waveform showed a 34.1% difference from the analytical results, the FFT analysis indicated that the torque order and harmonic components generally aligned with the theoretical predictions. This discrepancy is expected to be attributed to manufacturing challenges.**

***Index Terms*—torque ripple suppression, IPMSM, radial force, eddy current, magnetic coupling.**

I. Introduction

IPMSM is widely adopted in automotive and home appliance applications, primarily due to its superior efficiency and high power density. Nevertheless, their operating principles lead to the generation of torque ripple [1], which is a periodic pulsation of torque. This phenomenon contributes to increased motor vibration and noise, concurrently degrading the responsiveness of speed and position control systems. To mitigate this issue, previous research has been conducted, exploring various torque ripple suppression strategies from both structural and control perspectives. From a structural perspective, research has been conducted on fractional slot winding and skew structures [2], while from a control perspective, research has been conducted on control methods based on torque ripple estimation formulas using motor equipment constants [3]and on reduction methods using harmonic current injection [4]. However, existing methods still have issues such as increased costs, design constraints, and accuracy limitations, and there is currently no revolutionary torque ripple suppression technology that can solve all these issues at once.

The authors have proposed a new approach for the passive suppression of the IPMSM torque ripple utilizing the MPRS [5]. In this method, MPRS is mounted coaxially on the output shaft of IPMSM, and the torque ripple generated by IPMSM is passively canceled out by the torque generated by the MPRS. This method has many advantages. Specifically, it does not require complex external control, can be applied to any motor in principle, and can be used in combination with conventional suppression methods. Prior magnetic field analyses conducted by the authors have demonstrated that by designing MPRS to match the specific order, phase, and amplitude of the target torque ripple, a suppression effect of 59.2% in peak-to-peak value and 97.4% for specific torque ripple orders can be achieved. This preliminary study focused on basic verification of whether the proposed method is effective as theoretically predicted, and was limited to a simple evaluation of static torque characteristics in magnetic field analysis.

This paper reports the results of a multifaceted evaluation conducted to thoroughly examine the practicality of MPRS. Eddy current losses occurring within the MPRS were quantitatively evaluated using three-dimensional finite element analysis, and their impact on motor efficiency was clarified. In addition, the amplitudes of the radial force pulsations generated by the MPRS and IPMSM were calculated and compared to evaluate the impact of MPRS installation on electromagnetic vibration and noise. In addition to these analytical considerations, a prototype MPRS was manufactured, and its static torque characteristics were also verified.

II. Suppression Principle of The Proposal Method [5]

This chapter explains the structure of the MPRS, its suppression principle, and the suppression conditions. First, the suppression principle of the proposed method and the structures of MPRS and IPMSM are shown in Fig. 1. The MPRS is a device proposed with a focus on the decoupling phenomenon

Identify applicable funding agency here. If none, delete this.

seen in power transmission devices called magnetic couplings [6]. A typical magnetic coupling consists of two rotating parts, a drive part and a driven part, each of which has a permanent magnet. When the drive part rotates due to torque from the power source, the driven part rotates in synchronization with the drive part due to the attractive and repulsive forces of the permanent magnets, thereby transmitting power. During power transmission, if an excessive load is applied to the driven part and the synchronization between the driving part and the driven part is lost, periodic torque pulsation corresponding to the rotational angle occur between the two parts. This is the decoupling phenomenon. The proposed suppression method utilizes this decoupling phenomenon. The outer magnet, which corresponds to the driven part of the MPRS, is fixed to the motor case. The inner magnet, which corresponds to the driving part, is mounted on the shaft side of the IPMSM and rotates in synchronization with the IPMSM rotor. This structure intentionally induces the decoupling phenomenon between the fixed outer magnet and the rotating inner magnet. The periodic torque pulsation generated when the decoupling phenomenon occurs is adjusted to be in the opposite phase of the IPMSM torque ripple, thereby offsetting both torque ripples.

The torque ripple of IPMSM (T_{IPMSM}) and MPRS (T_{MPRS}) can be formulated as a Fourier series expansion of the rotor's rotational angle θ (mechanical angle), as shown in Equations (1) and (2) respectively. Here, T_{DC} is the commutation torque, A is the amplitude, P is the number of poles, ϕ is the phase difference (mechanical angle), and k is a natural number.

$$T_{\mathrm{IPMSM}} = T_{\mathrm{DC}} + \sum_{k=1}^{n} A_{\mathrm{IPMSM}k} \cos\left(\frac{P_{\mathrm{IPMSM}}}{2} 6k\theta + \phi_{\mathrm{IPMSM}k}\right) \tag{1}$$

$$T_{\mathrm{MPRS}} = A_{\mathrm{MPRS}} \cos\left(\frac{P_{\mathrm{MPRS}}}{2}\theta + \phi_{\mathrm{MPRS}}\right) \tag{2}$$

For torque ripple suppression, the orders of both torque ripples must be equal. Therefore, equation (3) below becomes the condition equation.

$$6P_{\mathrm{IPMSM}}k = P_{\mathrm{MPRS}}. \tag{3}$$

Furthermore, their phases must be in opposite phase (180-degree phase difference). Thus, equation (4) below becomes the condition equation.

$$\phi_{\mathrm{IPMSM}k} = \phi_{\mathrm{MPRS}} - \pi. \tag{4}$$

Additionally, to achieve a higher torque ripple suppression effect, the amplitudes of both components should be as close as possible. Therefore, equation (5) below becomes the condition equation.

$$A_{\mathrm{IPMSM}k} - A_{\mathrm{MPRS}} \to 0. \tag{5}$$

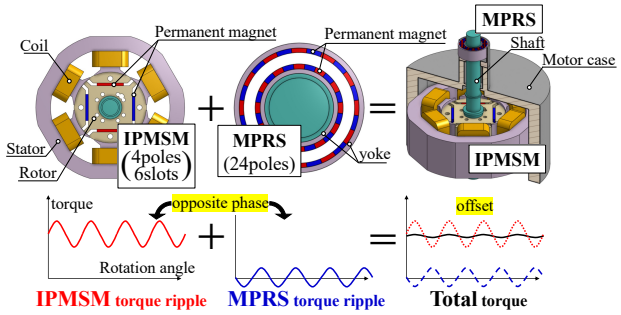

Fig. 1. Torque ripple suppression principle and MPRS and IPMSM structure

III. Analysis and Evaluation of MPRS Dynamic Characteristics

A. Method of Eddy Current Loss Analysis

Since MPRS utilizes the phenomenon of demagnetization, an alternating magnetic field is generated inside the permanent magnet, which may cause eddy current losses. Therefore, in this section, the effect of these eddy currents on motor efficiency was evaluated using three-dimensional finite element analysis. The analysis focused solely on the interior of the permanent magnet where magnetic flux changes are significant. The specifications and magnetic field analysis model of MPRS are shown in Table I and Fig. 2. Note that the skin depth of the permanent magnet was calculated to be approximately 30 mm based on the rotational speed, the magnetic permeability, and the electrical resistivity of the MPRS. Since this depth is sufficiently deep compared to the 1 mm thickness of the MPRS permanent magnet, the influence of the skin effect on eddy currents was ignored in the analysis.

TABLE I
Specifications of MPRS

Parameters (Unit)	Values
Number of poles	24
Residual flux density of permanent magnet (T)	1.4
electrical resistivity of permanent magnet ($\Omega \cdot$ m)	1.4×10^{-6}
permeability of permanent magnet (H/m)	1.32×10^{-6}
rotor rotational speed (RPM)	1500

B. Results of Eddy Current Loss Analysis

The analysis showed that the average value of eddy currents generated in the MPRS was 1.9 mW. For comparison, Table II shows various losses of the D1 model (IPMSM) published by the institute of electrical engineers at 1500 rpm [7]. From these results, it is clear that the eddy current loss generated in the MPRS is extremely small, at approximately 0.04% compared to the iron loss generated in the IPMSM. This can

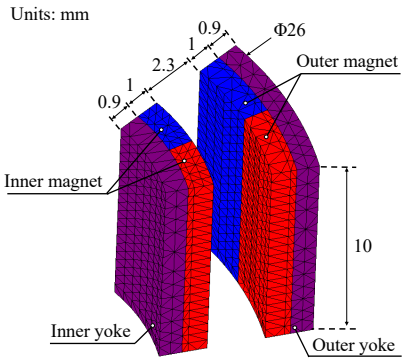

Fig. 2. magnetic field analysis model of MPRS

be attributed to factors such as the MPRS's small volume, which is only about 0.9% of the IPMSM's, and the fact that, due to its operating principle, the MPRS, unlike the IPMSM, does not experience magnetic flux reversal in its magnetic yoke and permanent magnets, leading to lower hysteresis loss. Furthermore, since the MPRS does not require current and has no mechanical contact, copper losses and mechanical losses do not occur. These results suggest that the motor efficiency does not decrease significantly even when the MPRS is installed.

TABLE II
EACH LOSS OF IPMSM [7]

	IPMSM	**MPRS**
Iron loss	4.53 W	1.9 mW
Copper loss	25.36 W	0 W
Mechanical loss	4.4 W	0 W
Total loss	34.3 W	1.9 mW

C. Method of Radial Force Analysis

In MPRS, among the forces acting between the outer magnet and the inner magnet, the circumferential components of magnetic attractive and repulsive forces become torque, while the radial components are unnecessary forces that do not contribute to torque. This unnecessary force is called the radial force, and its pulsation generates electromagnetic vibration, which ultimately causes noise. Radial force pulsation occurs not only in MPRS but also in IPMSM, contributing to noise [8].

In this section, to evaluate the impact of MPRS on vibration and noise, the three-dimensional finite element analysis was used to calculate the electromagnetic forces acting on the inner magnet surface of MPRS and the U-phase tooth surface of IPMSM (highlighted in purple in Fig. 4). The analysis models for IPMSM are shown in Fig. 3, and the specifications are shown in Table III. The MPRS analysis model is the same as in the previous section. To calculate the radial force of the MPRS, the radial force was determined when the rotor was forcibly rotated in increments of 0.5 degrees from 0 to 30 degrees, for a total of 61 steps. In the analysis domain, air was assigned to the shaft and motor case, but detailed consideration of these materials is left as a future task and is omitted in this paper. Considering rotational symmetry, a 1/12 partial model corresponding to one pole pair was used for the 24-pole MPRS. The IPMSM analysis model was constructed based on the D1 model of the Institute of Electrical Engineers of Japan [7]. The radial force of the IPMSM was calculated by forcibly rotating the rotor in a mechanical angle from 0 degrees to 180 degrees in increments of 1.8 degrees over 101 steps. Considering rotational symmetry, a 1/2 partial model corresponding to one pole was used. The number of elements in the three-dimensional mesh used for analysis was 93,908 for the MPRS and 177,200 for the IPMSM. The analysis time was 1 hour and 38 minutes for the MPRS and 3 hours and 30 minutes for the IPMSM.

TABLE III
SPECIFICATIONS OF MPRS

Parameters (Unit)	**Values**
Number of poles	4
Number of stator slots	6
Number of phase	3
Number of coil turns (per teeth)	125
Maximum voltage (V)	165
Maximum current (A)	7.5
Rated current (Arms)	4.4
Rated torque (Nm)	1.8
Coil resistance (per phase) (Ω)	0.380
Residual flux density of permanent magnet (T)	1.2

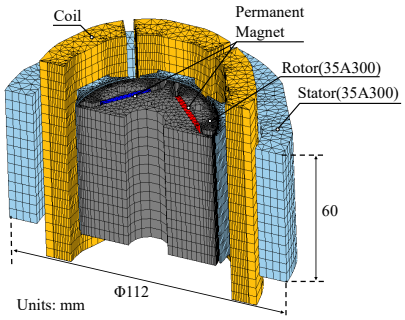

Fig. 3. magnetic field analysis model of IPMSM

D. Results of Radial Force Analysis

The radial force waveforms of IPMSM and MPRS obtained by magnetic field analysis and their FFT results for each are shown in Fig. 4. The radial force generated in MPRS is dominated by the sixth harmonic component at a mechanical angle of 180 degrees, which corresponds to the number of poles of MPRS. On the other hand, the radial force generated in IPMSM was dominated by the second harmonic component at a mechanical angle of 180 degrees. When comparing the amplitude of the main harmonic component of the radial force generated in the IPMSM with that generated in the MPRS, it was found that the latter is very small, approximately 6% of the former. Electromagnetic vibration and noise caused by radial forces are greatly affected by resonance with eigenmodes [9],

but based on these results, it is predicted that the electromagnetic vibration and noise generated by the installation of the MPRS will be sufficiently small compared to that of the IPMSM.

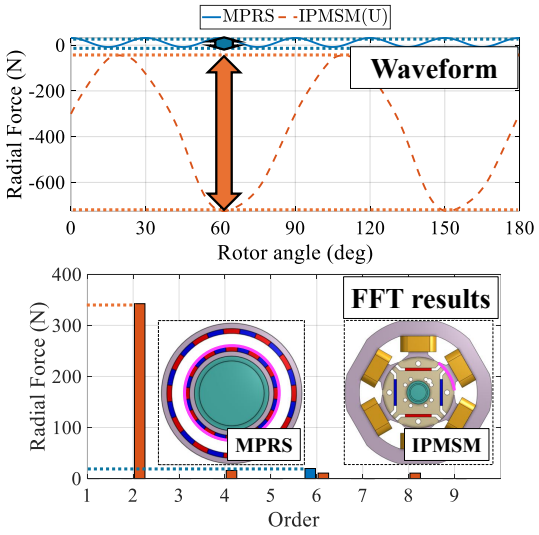

Fig. 4. Radial force analysis results of MPRS and IPMSM

IV. Prototype Validation

A. Method of Torque Measurement for prototype MPRS

In previous chapters, the effectiveness and practicality of the torque ripple suppression method using MPRS were evaluated in an ideal environment through computer-based analysis. In this chapter, the practicality of MPRS will be demonstrated by measuring the torque using a prototype MPRS. The aim is to verify whether the same torque as obtained in the aforementioned analysis can be obtained. A measurement system was constructed to evaluate the static torque characteristics of the MPRS prototype. The overall appearance of the system is shown in Fig. 5. When constructing the prototype MPRS device, the dimensions of the MPRS differed slightly from those in the aforementioned analysis. In addition, guides for positioning the permanent magnets were installed on the outer yoke and inner yoke of the MPRS. In order to compare the results of the physical device with those of the magnetic field analysis, a new magnetic field analysis model of the MPRS was also created with the same dimensions as the constructed device. The dimensions of the constructed MPRS are shown in Fig. 6. The MPRS case was prototyped using a 3D printer. As will be discussed later, it is expected that the rigidity of the material and dimensional accuracy are expected to negatively impact the measurement results. Therefore, a change to other non-magnetic materials is planned for the future. In addition, the permanent magnet, yoke, and case of the MPRS were manually bonded with an adhesive mainly composed of α-cyanoacrylate. For torque measurement, a torque meter (rated torque 1 N$\cdot$m, minimum resolution 1 mN$\cdot$m, rated rotational speed 6000 r/min) was used, with the input shaft of the torque meter connected to the outer case of the MPRS. An encoder-equipped servo motor was used as the drive source to rotate the inner magnet. Considering the periodicity of the MPRS torque, the system was rotated in 0.1-degree increments over a 15-degree range corresponding to half a torque cycle. In addition, a powder brake was connected to the output shaft of the torque meter to apply a load to the outer magnet of the MPRS and induce the decoupling phenomenon. The input current of the powder brake was set to 0.4A to generate a braking force of 6N, which is sufficiently bigger than the torque of the MPRS (0.21N) calculated by magnetic field analysis, so that the MPRS would constantly induce the decoupling phenomenon. The measurement was performed at a room temperature of approximately 25°C. The materials used for the Inner permanent magnets, Outer permanent magnets, case and shaft, and yoke of the MPRS were N42SH, N35SH, Polylactic Acid, and SS400, respectively. All of the above devices were fixed to the same optical table with screws to prevent positional shifts during measurement.

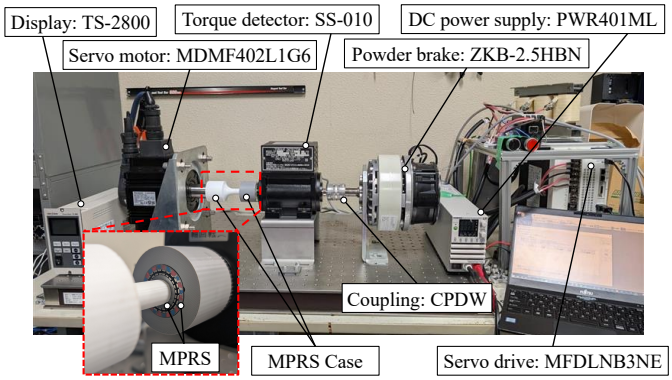

Fig. 5. Overall appearance of the Torque Measurement system

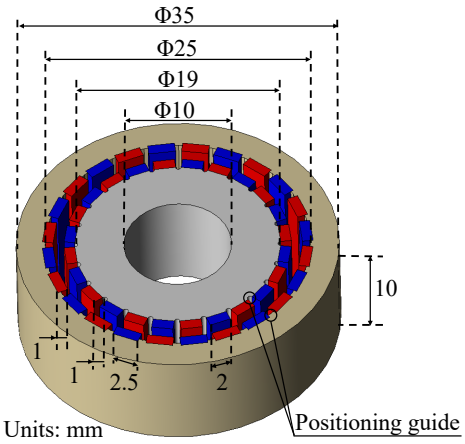

Fig. 6. MPRS magnetic field analysis model with the same dimensions as the manufactured MPRS

B. Results of prototype MPRS Torque

The static torque waveform of the prototype MPRS measured under the aforementioned conditions and the FFT results

are shown in Fig. 7. And the static torque waveform of MPRS under ideal conditions in magnetic field analysis and its FFT results are shown in Fig. 8. The measured torque waveform exhibited an amplitude difference of 34.1% compared to the analytical results predicted during the design phase. Furthermore, the FFT results of the measured torque confirmed that the torque order and harmonic components generally correspond with theoretical characteristics. Several factors are believed to be the primary reasons for the 34.1% difference in torque amplitude and the slight presence of the 3rd-order harmonic component. These include the imperfect alignment of the MPRS's inner and outer shafts, which leads to a non-uniform air gap width. Another factor is the manual bonding of the MPRS's permanent magnets, resulting in irregular spacing between each of them. Additionally, the insufficient rigidity of the MPRS's shaft, made of Polylactic Acid, causes eccentricity. The FFT results indicate that the MPRS can be used to suppress torque ripple. However, more precise manufacturing and installation of MPRS are necessary to achieve greater suppression effectiveness.

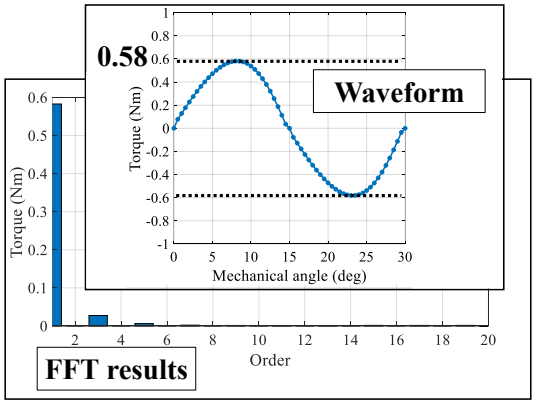

Fig. 7. The static torque waveform of the prototype MPRS and its FFT results

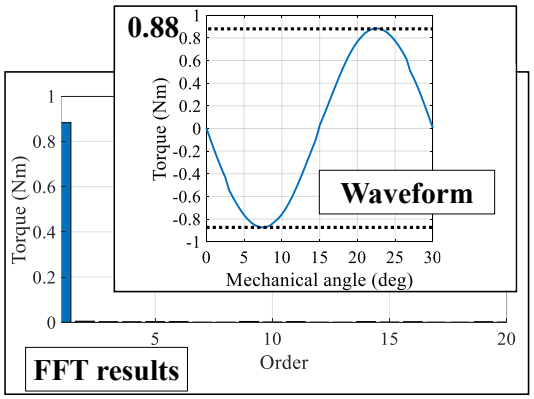

Fig. 8. The static torque waveform of the MPRS in magnetic field analysis and its FFT results

V. Conclusion

In this paper, the practicality of a new method for suppressing torque ripple in AC motors using MPRS was evaluated. Through three-dimensional finite element analysis, it was confirmed that the eddy current loss of the MPRS is extremely small, accounting for approximately 0.04% of the iron loss of the IPMSM. This result indicates that integrating the MPRS does not significantly reduce motor efficiency. Additionally, since the radial force amplitude is also very small, at approximately 6% of that of an IPMSM, it is predicted that the installation of the MPRS will result in minimal increases in electromagnetic vibration and noise. In prototype validation, the amplitude of the measured static torque waveform showed a difference of 34.1% from the analysis results, but the FFT results confirmed that the order and harmonic components of the torque were generally in line with theory. The difference in amplitude is thought to be caused by manufacturing issues such as uneven shaft alignment, manual bonding of permanent magnets, and eccentricity due to insufficient shaft rigidity.

In conclusion, multiple results suggest that MPRS is effective in suppressing torque ripple. However, to maximize its suppression effect, precise manufacturing and installation techniques are essential. Future work will focus on reducing the discrepancy in torque amplitude between experimental and analytical results by improving the manufacturing and installation precision of the MPRS and by modifying the shaft material. Subsequently, the MPRS will be installed on a motor to verify its suppression effectiveness.

Acknowledgment

This work was supported by JSPS KAKENHI Grant Number 24K17254.

References

[1] P. Yi, W. Zheng and X. Li, "Overview of Torque Ripple Minimization Methods for Permanent Magnet Synchronous Motors Based on Harmonic Injection, "Chinese Journal of Electrical Engineering, Vol. 10, No. 2, pp. 16-29, 2024.

[2] T. Takano, "Optimization of Skew Angle for Cogging Torque Reduction," DENKI-SEIKO, vol. 82. No. 1, pp. 67-72, 2011.

[3] N. Nakao and K. Akatsu, "Torque Ripple Control Based on Instantaneous Torque Estimation in PMSMs," IEEJ Transactions on Industry Applications, Vol. 131, No. 9, pp. 1020-1127, 2011.

[4] G. H. Lee et al., "Torque Ripple Reduction of Interior Permanent Magnet Synchronous Motor Using Harmonic Injected Current," IEEE Transactions on Magnetics, Vol. 44, No. 6, pp. 1582-1585, 2008.

[5] H. Ito, and M. Kato, "Torque Ripple Suppression in AC Motor Using Magnetic Periodic Reversal Spring," Proceedings of the 21st Biennial Conference on Electromagnetic Field Computation (CEFC), pp. 1-2, 2024.

[6] K. Sakai, T. Oishi, T. Tokumasu, and Y. Tagawa, "Torque Analysis of Large Permanent Magnet Coupling," IEEJ Transactions on Fundamentals and Materials, Vol. 113-A, No. 4, pp. 313-320, 1993.

[7] "Investigating R&D Committee on Practical Analysis Technique of 3-D Electromagnetic Field for Rotating Machines," IEEJ Technical Reports, No. 1296, 2013.

[8] X. Rao et al., "Investigation of Noise Sources in Fractional-Slot Concentrated Winding Motors Considering High-Order Radial/Tangential Electromagnetic Force Combination and Modulation," IEEE Access, Vol. 11, pp. 143980-143997, 2023.

[9] N. Niguchi, K. Hirata, T. Kondo, "Resonant Characteristics of Electromagnetic Vibration of an Electric Power Steering Motor," IEEJ Transactions on Industry Applications, Vol. 133, No. 10, pp. 1022-1030, 2013.